DOE FINAL REPORT

Energetics of Nanomaterials

Award Number: DE-FG03-01ER15235
Work Done at BYU: 9/1/01 – 10/31/04

This project, "Energetics of Nanomaterials", represents a three-year collaboration among Alexandra Navrotsky (University of California at Davis), Brian Woodfield and Juliana Boerio-Goates (Brigham Young University) and Frances Hellman (University of California at San Diego but moving to University of California at Berkeley). Its purpose has been to explore the differences between bulk materials, nanoparticles, and thin films in terms of their thermodynamic properties, with an emphasis on heat capacities and entropies, as well as enthalpies. The three groups have brought very different expertise and capabilities to the project. Navrotsky is a solid-state chemist and geochemist, with a unique Thermochemistry Facility emphasizing enthalpy of formation measurements by high temperature oxide melt and room temperature acid solution calorimetry. Boerio-Goates and Woodfield are physical chemists with unique capabilities in accurate cryogenic heat capacity measurements using adiabatic calorimetry. Hellman is a physicist with expertise in magnetism and heat capacity measurements using microscale "detector on a chip" calorimetric technology that she pioneered. The overarching question of our work is "How does the free energy play out in nanoparticles?" or "How do differences in free energy affect overall nanoparticle behavior?" Because the free energy represents the temperature-dependent balance between the enthalpy of a system and its entropy, there are two separate, but related, components to the experimental investigations: Solution calorimetric measurements provide the energetics and two types of heat capacity measurements the entropy. We use materials that are well characterized in other ways (structurally, magnetically, and chemically), and samples are shared across the collaboration.

We are using these combined techniques to address the following questions: How does energy and entropy depend on particle size? Do entropic differences have their origins in changes in vibrational densities of states or configurational (including surface configuration) effects? Do material preparation and sample geometry, i.e., nanoparticles versus thin films, change these quantities? How do the thermodynamics of magnetic and structural transitions change in nanoparticles and thin films? Are different crystal structures stabilized for a given composition at the nanoscale, and are the responsible factors energetic, entropic, or both? How do adsorption energies (for water and other gases) depend on particle size and crystal structure in the nanoregime? What are the energetics of formation and strain energies in artificially layered thin films? Do the differing structures of grain boundaries in films and nanocomposites alter the energetics of nanoscale materials?

Of the several directions we first proposed, we initially concentrated on a few systems: TiO_2, CoO, and CoO-MgO. These have been experimentally controllable, amenable to our suite of techniques, and represent good model systems that are relevant to technological and geochemical applications as well as to the fundamental underlying science. The main body of the proposal below discusses progress during the current grant and proposed new work. The latter includes both the continuation of studies underway and new directions for the next four years. Each subsection is organized to highlight the state of the art at the beginning of the grant, what we have learned, and work to be performed.

The present collaboration has been very congenial and fruitful. We have exchanged both samples and scholars among the laboratories. In particular, Lan Wang and Juraj Majzlan from UCD each spent several months at BYU. We have met, often bringing our students and postdocs, as well as the PIs, several times a year, rotating these meetings among the three institutions. We have had even more frequent conference calls and are in constant email contact. We work extremely well as a team. We have learned an immense amount from each other because we bring not just different methodologies but different disciplines to the project. In particular, the interplay of physics (Hellman), chemistry (Woodfield, Boerio-Goates, Navrotsky) and geochemistry (Navrotsky) viewpoints has been very enriching. Hellman moved from San Diego to Berkeley several months ago.

This report summarizes the work at all tour institutions and is being submitted by all the PIs.

PUBLICATIONS FROM GRANT

Published

J. Majzlan, A. Navrotsky, B. F. Woodfield, B. E. Lang, J. Boerio-Goates, and R. A. Fisher Phonon, spin-wave, and defect contributions to the low-temperature specific heat of α-FeOOH. *J. Low Temp. Phys*. **130**, 69-76 (2003).

J. Majzlan, B. E. Lang, R. Stevens, A. Navrotsky, B. F. Woodfield, and J. Boerio-Goates, Thermodynamics of Fe Oxides: Part I. Entropy at standard temperature and pressure and heat capacity of goethite (α-FeOOH), lepidocrocite (γ-FeOOH), and maghemite (γ-Fe_2O_3). *Am. Mineral.* **88**, 846-54 (2003).

B. Revaz, D. O'Neil, L. Hull, and F. Hellman, Numerical Simulation of the Heat Transfer in a-Si-N-Membrane Based Microcalorimeters, *Rev. Sci. Instr*. **74**, 4389 (2003).

L. Wang, A. Navrotsky, R. Stevens, B. F. Woodfield, J. Boerio-Goates, Thermodynamics of CoO-MgO solid solutions. *J. Chem. Thermodynam*. **35**, 1151-1159 (2003).

Y. J. Tang, D. J. Smith, B. L. Zink, F. Hellman, and A. E. Berkowitz, Finite size Effects on the moment and ordering temperatures in antiferromagnetic CoO layers. *Phys. Rev. B.* **67**, 054408 (2003).

G. Li, L. Li, J. Boerio-Goates, B. F. Woodfield, Grain growth kinetics of rutile TiO_2 nanocrystals under hydrothermal conditions. *J. Mater. Res.* **18**, 2664-2669 (2003).

Forray, F.L., Navrotsky, A., Drouet, C., (2004) Jarosite stability on Mars, Second Conference on Early Mars: Geologic, Hydrologic, and Climatic.

Evolution and the Implications for Life. October 11-15, 2004, Jackson Hole, WY, Abstract #8009. Lunar and Planetary Institute, Houston (CD-ROM).

In Press or Submitted

G. Li, L. Li., J. Boerio-Goates, B. F. Woodfield. Linear lattice expansion and covalency enhancement in rutile TiO_2 nanocrystals. Submitted to *Appl. Phys. Let.*

L. Wang, A. Navrotsky, R. Stevens, B. F. Woodfield and J. Boerio-Goates, Calorimetric study: surface energetics and the magnetic transition in nanocrystalline CoO. *Chem.Mater. (in press)*

G. Li, L. Li, J. Boerio-Goates, B. F. Woodfield. Synthesis and grain growth kinetics of highly pure anatase TiO2 nanocrystals by a sol-gel method. Submitted to *J. Mat. Res*.

Forray, F.L., Drouet, C., Navrotsky, A., (2005) Thermochemistry of yavapaiite KFe(SO4)2: Formation and decomposition. Geochim. Cosmochim. Acta, in press.

Navrotsky, A., Forray, F.L., Drouet, C., 2005. Jarosite stability on Mars. Icarus, submitted

In Preparation

J. Boerio-Goates, R. Stevens, T. Walker, B. F. Woodfield, L. Wang and A. Navrotsky, Heat capacities and thermodynamic functions of CoO, MgO and $Co_{0.50}Mg_{0.50}O$,. In preparation for *J. Chem. Thermodynamics*

J. Boerio-Goates, R. Stevens, B. F. Woodfield, R. A. Fisher, L. Wang and A. Navrotsky, An analysis of the magnetic and electronic contributions to the specific heat of single crystal CoO. In preparation for *Phys. Rev. B.*

PEOPLE SUPPORTED ON GRANT

Name	***Institution/Position***	***Project***	***Present Position***
Lan Wang	UCD postdoc	CoO-MgO bulk, nano	UCD
Andrey Levchenko	UCD postdoc)	TiO_2	UCD
Juraj Majzlan	Davis PhD 02	iron oxides	Princeton postdoc
Yunjun Tang	UCSD postdoc	CoO films, multilayers	UCSD
Daniel Queen	UCSD grad student	CoO film Cp	UCSD/UCB
David Cooke	UCSD grad student	High T calorimetry	UCSD/UCB
Richard Pietri	UCSD postdoc	He^3 calorimetry	Desert Cryogenics
Guangshe Li	BYU postdoc	TiO_2 synthesis	Fujian Inst. Research
Shengfung Liu	BYU postdoc	Cp	BYU
Brian Lang	BYU PhD 04	Cp, apparatus const.	BYU
Rebecca Stevens	BYU MS 03	Cp	Cal Tech grad student
Jeffrey Boyer	BYU undergrad	Cp	U. Wash. Med. School
Marcus Donaldson	BYU undergrad	Cp	UCB grad.student
Sara Doot	BYU undergrad	Cp	BYU

Trent Walker	BYU undergrad	Cp	BYU
Aaron Lewis	BYU undergrad	Cp	Wisconsin Med College
Tyler Meldrum	BYU undergrad	Cp	BYU
Thomas Parry	BYU undergrad	Cp	BYU

TiO_2 AT THE NANOSCALE

The phases of TiO_2 (rutile, anatase, brookite) are an excellent system to study the interplay of polymorphism, particle size, and hydration. Our goal has been to study these effects on enthalpy, heat capacity, entropy, and free energy, and to link these properties to a molecular-level understanding of structure and bonding. We realized at the beginning of this project that obtaining a suite of well-defined materials with controlled chemistry, particle size, and water content was a crucial first step of our studies. This has been a larger focus of the project than initially envisioned but it has paid off well yielding both fundamental understanding and excellent samples for experiments.

Synthesis and coarsening kinetics

Recognizing the importance of well-characterized samples, we have developed and improved upon several synthetic methodologies that allow us to produce both phase pure and chemically pure nanoparticles. First, using a hydrothermal technique we synthesized rutile nanorods with high crystallinity by starting with the hydrolysis of $TiCl_4$ and we used a modified sol-gel method to obtain high quality spherical anatase nanoparticles. Details can be found in our publication [Li 2003].

Secondly, we have produced nanoparticles free of adsorbed chlorine or organic species. Rutile nanorods and anatase nanospheres were achieved in 40 g quantities with extremely low impurities by numerous washings of the reaction samples using a centrifuge until the pH of the wash solution was approximately 7. The resulting rutile and anatase nanoparticles were white; analysis by a commercial laboratory found only carbon and chlorine at the ppm level in both samples.

Thirdly, we characterized the samples extensively using a variety of techniques, including: (i) XRD, which showed single-phase rutile and anatase nanoparticles, (ii) TEM, which clearly showed that rutile nanoparticles are rod-shaped and anatase nanoparticles are spherical with uniform size distributions. (iii) Various wet and dry chemical analyses, which showed impurities only on the ppm level. (iv) TG-DSC, which showed that both TiO_2 nanoparticles dehydrated over a wide temperature range to about 750 °C and quantified the water content of the samples as a function of particle size (see below). (v) EPR, which showed the absence of Ti^{3+} in both rutile and anatase samples. (vi) Raman, which gave the standard spectra for single phase anatase or rutile but showed systematic shifts in Raman mode frequencies with increasing particle size (see Section 4.4). (vii) IR, which showed the presence of hydration layers in TiO_2 nanoparticles (the size of the hydration layers become larger with decreasing particle size, consistent with our TG-DSC measurements). (viii) BET, which gave surface areas consistent with our XRD and TEM results.

We have also been able to develop improved models that describe the grain growth kinetics for TiO_2 nanoparticles, giving us precise control of the particle sizes. Using $TiOCl_2$ as the starting material (d_0 = 0), we obtained rutile nanoparticles in a single step with temperature, T, and reaction time, t, as two effective variables to control the particle sizes. The rutile particle size (rod diameter), D, and t follow the relationship $\ln D = 2.74(4) + 0.20(2)\ln t$ (see Figure.1). We also found a linear relationship between ln (D) and T, $\ln D = 11.5(3) - 4.1(1)\times 10^3 / T$. Combining both equations, we obtained a generalized model for the grain growth kinetics of rutile nanocrystals under hydrothermal conditions, $D^5 = 6.94\times 10^{24}\cdot t\cdot e^{(-E_a/RT)}$ where E_a = 170.8 kJ/mol.

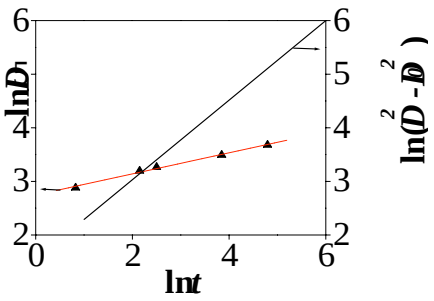

Figure1. *Rate of grain growth for rutile TiO_2 nanoparticles.* ▲*BYU; — [Hofler 1990]. Work done at BYU.*

The grain growth kinetics for anatase nanoparticles synthesized using a sol-gel method can be significantly different from those synthesized using hydrothermal methods or vapor

condensation. We found that the grain growth kinetics starting with 7nm anatase nanoparticles could be well fitted to the following equation: $D^2 - D_0^2 = k_0 \cdot t^n \cdot e^{(-E_a/RT)}$ where n = 0.286(9) and E_a = 32(2) kJ/mol. We note that this activation energy is substantially smaller than for any model of grain growth in anatase nanoparticles reported previously.

Effect of particle size and water content on vibrational heat capacities of nano-TiO_2 polymorphs

We have measured the *Cp* of well-characterized bulk samples of rutile and anatase from 0.6 to 400 K to provide a complete baseline for comparison with our nanoparticles since there are discrepancies in the reported heat capacity of rutile and no experimental measurements on anatase below 50 K. Having good baselines for the bulk material below 50 K is imperative since it is here that one would expect to see significant contributions from low energy modes such as those predicted by the Wolf model. Also, low-temperature heat capacity effects contribute more significantly to the entropy at 298 K and may be important to the surface entropy of the nanoparticles.

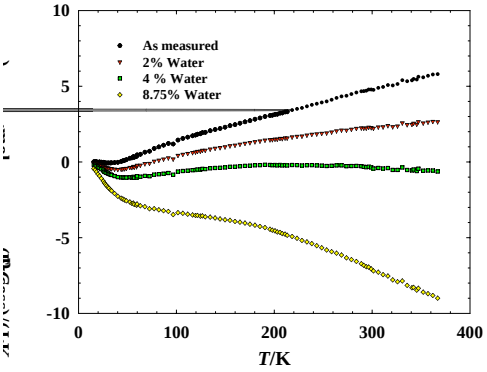

Figure 2 *Excess heat capacity of rutile nanoparticles corrected for different weight % of water.* • *as measured;* □ *2% ;* ◇ *4%;* ⊄ *8.75%. Work done at BYU.*

Early on, we realized the extent to which the adsorbed water can influence the apparent excess heat capacity. Figure 2 shows how C_{excess} of 8 nm rutile sample changes as corrections for water are made. The uncorrected "as measured" C_{excess} (the quantity reported by most authors in studies of nanoparticles) has an excess of about 5 J/K at 300 K. However, C_{excess} decreases as larger water corrections are made using *Cp* (ice,Ih) to model the water. Our calorimetric sample contained about 6 weight % water, so it would have a negative excess heat capacity. Thus, our work has shown that the "excess" heat capacity reported to date for many nanoparticles may be a result of unaccounted-for contributions from species such as water adsorbed on the surface.

Effect of particle size and water content on enthalpy of formation of TiO_2 polymorphs

At the start of the grant, Navrotsky's group [Ranade 2002] confirmed similar energy crossovers in titania, using a limited number of samples of rutile, anatase, and brookite (see Table 1 and Figure 3). The increase in metastability of the polymorph is paralleled by a decrease in surface energy, resulting in the energy crossovers seen in Figure 3

The samples for these studies came from several collaborators and were characterized to various extents. These data were based on a correction for water content based on the heat content of free water, that is, under the assumption that the water is loosely bound and similar in energetics to liquid water. Because the water in titania is evolved at much lower temperature than the water in alumina, this assumption is more reasonable for the former system. Nevertheless, we are refining these data using the larger suite of well-characterized samples we have prepared, and to evaluate the energetics of water adsorption. This work is in progress and preliminary findings are as follows.

Phase	*Enthalpy relative to rutile (kJ/mol)*	*Surface enthalpy (J/m^2)*
Rutile	0	2.2±0.2
Brookite	0.7±0.4	1.0±0.2
Anatase	2.6±0.4	0.4±0.2

Table 1 *Titania Energetics Data from [Ranade 2002]. Work at UCD.*

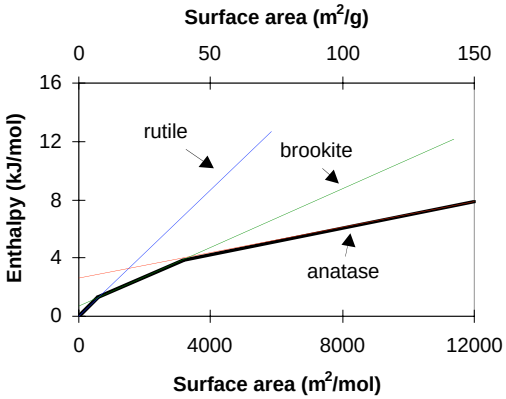

Figure 3. *Energetics of the TiO_2 polymorphs. Figure modified from [Ranade 2002]. The slope of each line gives the surface energy and its intercept the enthalpy of the coarse polymorph relative to rutile. Heavy line shows energetic stability regions of different phases. Work at UCD.*

We have begun solution calorimetry at Davis on the systematic set of samples of different particle size and water content prepared at BYU. 19 samples of pure anatase, synthesized at BYU, were sent to Davis for further characterization and calorimetry. The water contents obtained by TGA in a stepped regime and particle sizes from XRD are presented in Table 2. The transition enthalpy of 11 anatase samples relative to the most stable rutile phase have been studied by high temperature drop solution calorimetry using sodium molybdate solvent. The moisture-sensitive samples were kept in a glovebox under argon. Care was taken to minimize sample exposure to air (< 1.5 sec). The specific surface area was measured by BET. The TG curve for anatase (a12) (Figure 4) shows weight loss over a large temperature range, indicating a variety of bonding environments for the adsorbed water.

The enthalpies of drop solution, water contents (measured at Davis), BET surface area, and particle sizes (calculated from BET surface area) are summarized in Table.3. The TGA results from Davis and BYU are in good agreement. As expected for particles smaller than 20 nm, sizes obtained by both BET and XRD agree within error. It is likely that particles > 20 nm are polycrystalline, having smaller crystallographic domain size than particle size.

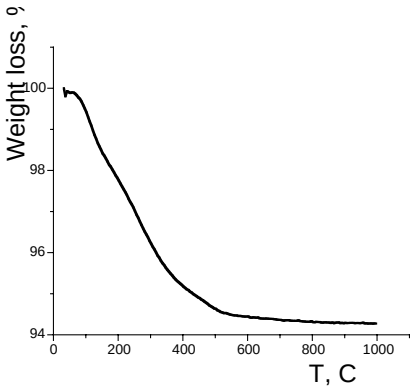

Figure 4. *TG curve for anatase (a12), measured at BYU.*

Sample ID	Particle size, XRD (nm)	Weight loss (%)
A0	7.7	9.84
A1	8.1	8.81
A2	9.3	6.74
A3	13.0	3.42
A4	16.8	2.05
A5	20.9	1.34
A6	28.9	0.70
A11	7.8	9.47
A12	9.1	6.95
A13	12.4	3.81
A14	17.1	1.99
A15	20.8	1.35
A16	28.2	0.73
A31	12.9	3.49
A32	13.3	3.28
A33	14.0	2.97
A34	17.0	2.01
A35	20.1	1.44
A36	27.7	0.76

Table 2. *Water contents, x, for the anatase nanoparticles $TiO_2.nH_2O$. Measurements at BYU.*

Table 3. *Sample characterization and thermochemical data for nanoanatase. Work at UCD*

Sample name	Surface area BET, m2/g	Particle size, BET, nm	Water content, %	ΔH_{ds} (corrected), kJ/mol	Uncertainty, kJ/mol	ΔH_{tr}, kJ/mol
a2	218	7.2	5.89	44.28	1.05	13.66
a3	114	13.7	2.94	51.10	1.14	6.85
a5	39	40.1	1.53	55.03	0.96	2.92
a6	37	42.7	0.99	55.59	1.06	2.35
a11	245	6.4	8.50	43.98	1.22	13.97
a12	207	7.5	5.67	44.48	1.18	13.47
a13	140	11.2	3.17	49.01	1.23	8.94
a14	70	22.3	1.81	53.49	1.20	4.46
a15	42	37.2	1.50	53.82	0.84	4.13
a16	31	50.4	1.17	55.63	1.03	2.32

The evolved gas analyses (Figure 5) show that the major component associated with the weight loss is water. The evolved gas FTIR confirms that water desorbs over a wide range of temperature, confirming the existence of some amount of chemically bound water.

The enthalpies of drop solution have been corrected for the moisture content in nanoparticles assuming loosely bound water. The water content ranges from 0.5 to 9 weight percent, which yields an enthalpy correction of 0.7 to 6 kJ/mol. Careful determination of water content is thus of crucial importance, as is characterization of the energetics of the more strongly bound water, to be done in the future. New preliminary calorimetric results for anatase are depicted in Figure 6.

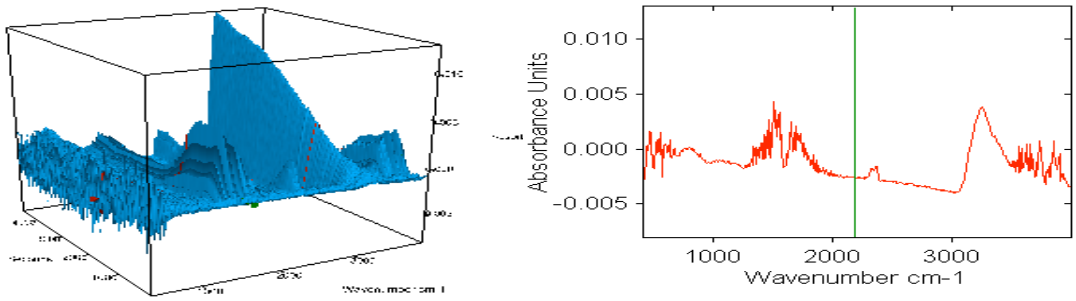

Figure 5. *Typical evolved gas FTIR spectrum for anatase (a11) Work at UCD.*

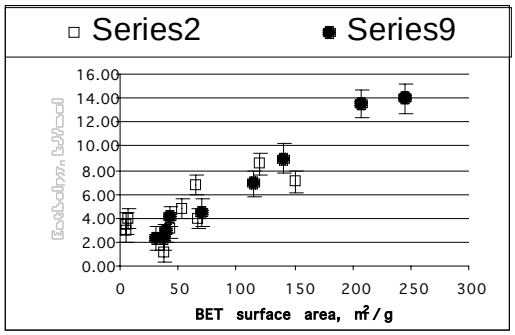

Figure 6. *Enthalpy of nanocrystalline anatase samples relative to bulk rutile vs. surface area. Work at UCD*

Surface hydration, unit cell volume, and dependence of vibrational frequency on particle size in TiO_2

We have studied the water content of rutile and anatase nanoparticles as a function of initial particle size, annealing temperature, and the resulting final particle size due to coarsening. The relationship between particle size, hydration, and temperature for rutile nanorods was examined and found to be well described by the expression $\frac{m}{m_o} = \frac{C}{DT^2} e^{(-E_a/RT)}$ where D is the initial particle size (rod diameter), T is the annealing temperature, m/m_o is the relative water mass with m_o being the mass of the sample before annealing, $C = e^{19.31(8)}$ and E_a = 0.35(1) eV (see Figure 7). For the anatase nanospheres, the surface hydration is a function of $1/D^2$ (sphere diameter) and can be represented by $\frac{m}{m_o} = \frac{C}{D^2T^2} e^{(-E_a/RT)}$ where $C = e^{22.0(1)}$ and E_a = 0.37(1) eV (see Figure 8). With these expressions, we are able to determine the annealing temperature that is needed to produce TiO_2 particles of a certain size and relative water content [Li, 2004]. It is clear from these results that the hydration layers on the TiO_2 nanoparticles stabilize particles on the nanoscale and act in a manner analogous to the "capping" by various organic molecules for other nanoparticle systems.

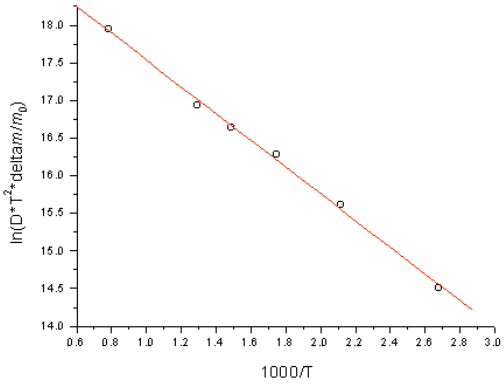

Figure7. *The relationship among the initial particle size, annealing temperature, and surface hydration for rutile nanorods. Work at BYU.*

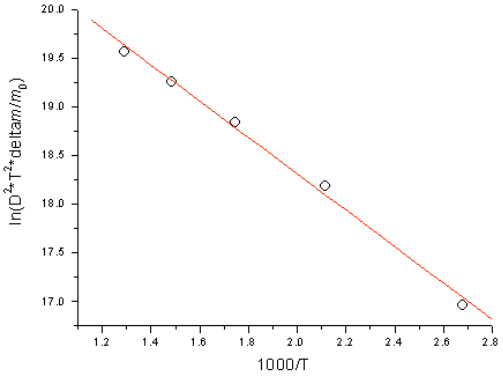

Figure 8. *The relationship among the initial particle size, annealing temperature, and surface hydration for anatase nanospheres. Work at BYU.*

We have also examined the size relationships of lattice volume (measured by X-ray diffraction) and the strongest E_g Raman frequencies of rutile and anatase nanoparticles. We first found that the lattice expansion in rutile is proportional to $1/D$ where D is the rod diameter (see Figure 9). It can be expressed as $V - V_0 = \frac{2.56(6)}{D}$, where V_0 is the unit cell volume for bulk rutile. A similar size dependence was also found for variations in the E_g Raman frequency, $v - v_0 = \frac{-28(2)}{D}$ where v_0 is the E_g mode frequency for bulk rutile. This lattice expansion has been explained in terms of the enhanced surface defect dipoles [Li, (2004)] that involve the contributions from the surface hydration bonding states as well as the spontaneous polarization in the nanoparticles.

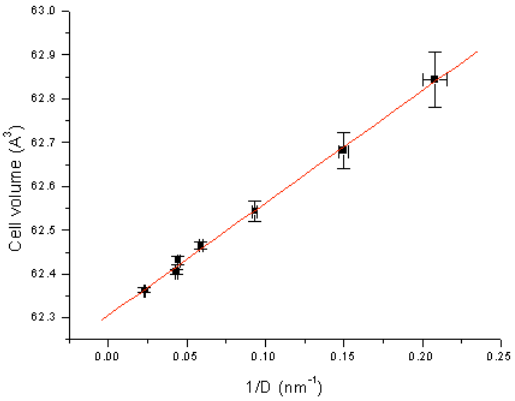

Figure 9*Unit cell volume as a function of particle size for rutile nanorods. Work at BYU.*

Surprisingly, we found that for the anatase nanospheres, the cell volume showed a decreasing trend. A

fit of the data gives an expression, $V - V_o = \frac{-99(5)}{D^2}$, where V_0 is the unit cell volume for bulk anatase. We also found that the Raman mode shifts are opposite to those for rutile and could be fit to the equation, $v - v_o = \frac{619(31)}{D^2}$, where v_0 is the E_g mode frequency for bulk anatase.

These expressions for the cell volume dependence and E_g mode shifts are surprisingly consistent. The $1/D$ size dependence for nanorod rutile and $1/D^2$ dependence for nanosphere anatase were also found for the grain growth kinetics and surface hydration expressions. Consequently, the $1/D$ dependence for rods and the $1/D^2$ dependence for spheres provide strong support that the surface area is the primary property governing grain growth, cell volume, and the primary phonon modes.

Effect of particle size on magnetic transitions in metallic oxides, particularly CoO.

Table 4 *Parameters extracted from low temperature Cp*			
Material	***H*/ Tesla**	**Linear Term/ mJ ·K^{-2} · mol^{-1}**	**Θ_D/K**
Single Crystal	46.1± 0.5	0.4 ± 0.1	518± 10
7 nm	43.5 ± 1.0	6.0 ± 0.2	225 ± 20

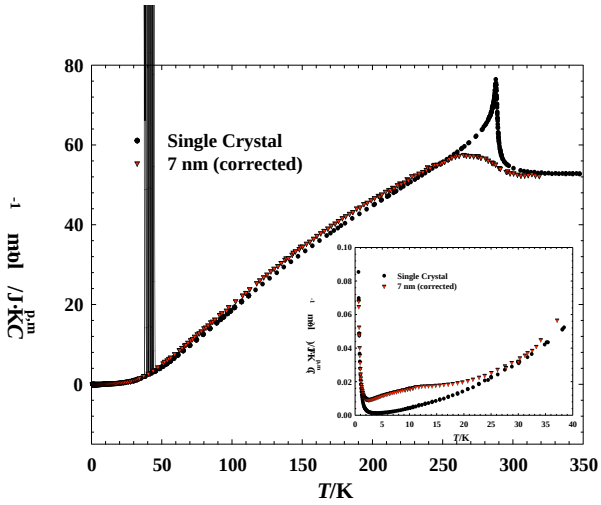

Figure 10 *The heat capacity of 7 nm CoO corrected for water and Co_3O_4,* •. *Single crystal CoO is included as a reference,* ♦. *Work at BYU*

CoO nanoparticles were prepared by the thermal decomposition of cobalt hydroxides in a hydrogen/argon atmosphere. They were characterized by XRD for phase purity and particle size, BET measurements for surface areas, SEM and TEM for particle morphology and size, TG for water and excess oxygen content, and electron microprobe for metals content. The particles were found to be (7.0 ± 1.0) nm with a surface area of (8921 ± 28) $m^2 \cdot mol^{-1}$. There was a broad peak in the XRD at low angle that could indicate the presence of amorphous material. The Co/O ratio and water content can be expressed as $CoO_{(1.043\pm0.001)}\cdot(0.094\pm0.002)H_2O$ or as $CoO\cdot(Co_3O_4)_{0.05}\cdot(H_2O)_{0.12}$ if the excess oxygen is present as Co_3O_4. As discussed above for the TiO_2 systems, water is a major component of these nanoparticles.

Figure 10 shows *Cp* of nano-CoO corrected for both water (as ice Ih) and Co_3O_4 using literature data. Our results for single crystal CoO are shown for comparison. The inset shows the low temperature results, plotted as *Cp*/*T* vs. *T*, for both samples. Below 15 K, a broad bump in the nanoparticle *Cp* is evident, particularly in the inset to Figure 10. Bulk Co_3O_4 has a magnetic transition near 30 K [Khriplovich, (1982)], but our corrections were only for the lattice. We take this bump as evidence for nano-Co_3O_4, which has been reported as a surface contaminant on nano-CoO [Soriano 1999].

A magnetic phase transition appears in the *Cp* of single crystal CoO as a λ-type anomaly with Néel temperature, T_N, = 287.78 K; the shape is characteristic of long-range magnetic ordering. The peak broadening seen in the nanomaterial implies that long-range spin order is destroyed, but short-range order remains, and with a characteristic energy that is largely unchanged since T_N has dropped by only about 20 K. This result is in agreement with the Hellman report, cited earlier, that the magnetic transition persists in CoO, and that the temperature at which short range ordering occurs (which dominates the thermodynamic signature) is not greatly diminished under conditions where long-range order cannot be achieved.

From an analysis of the low temperature *Cp* of CoO nanoparticles and crystals, we have extracted the magnitude of the internal field (also called the hyperfine field) *H* that splits energy levels of the Co-59 nucleus and leads to the upturn below 1 K (see inset to Figure 10), as well as the Debye temperatures Θ_D. Linear terms were needed in the analysis to accurately reproduce *Cp* for both materials. The results of the analysis are given in Table 5.1.1. We gain the following insights: (1) The large linear term in the nanoparticle *Cp* suggests either a significant degree of disorder in the nanoparticles or the presence of an amorphous component in the sample. Similar results from computer simulations, phonon theory and *Cp* measurements on nanocrystals of Pd have been reported. [Smith 1993; Wolf 1995; Shrivastava 2002; Oya 1999]. (2) The lower hyperfine field *H* in CoO nanoparticles indicates a decrease in the coupling between the electronic and nuclear spins. Mössbauer investigations on γ-Fe_2O_3 [Haneda

1977, 1987] and $BaFe_{12}O_{19}$ [Gajbhiye 1999] nanoparticles have also reported such reductions. (3) The greatly reduced Debye temperature of the nanoparticles indicates a softening of the phonons in the nanoparticles.

Using our single crystal results as a baseline, we have calculated C_{excess} for nano-CoO. Below 250 K, C_{excess} is positive, but it goes negative at higher temperatures because of the larger magnetic anomaly in the single crystal. The excess entropy of the nanoparticle ($S_{nano} - S_{crystal}$) is positive at all temperatures. At 250 K, the excess entropy is about 2.4 $J \cdot K^{-1} \cdot mol^{-1}$ and it drops to 1.5 $J \cdot K^{-1} \cdot mol^{-1}$ at 298 K. Taking the S_{excess} at 250 K as arising primarily from surface contributions, we calculate a surface entropy of 2.8 mJ $\cdot K^{-1} \cdot m^{-2}$, which is in excellent agreement with the result of Jura and Garland [Jura 1952] for MgO.

We have also measured the specific heat of vapor-deposited thin film CoO. In these films, there are two different structural lengths, each of which can be controlled; (1) film (or layer) thickness, which can be reduced easily to the nanometer regime and accurately prepared and measured, with very little dispersion (in a multilayer film); and (2) grain size for a polycrystalline film, which is controlled by growth conditions (substrate choice, growth temperature and rate, partial pressure, ion bombardment, growth technique) and any subsequent annealing. The nature of the grain boundaries and any interface structure control whether these grain boundaries limit the magnetic interactions (and less likely, the phonons). Hence films can be either 2 dimensional structures, limited by thickness, or can (at least in principle) exhibit 0D to 3D crossover effects.

Figure 11 shows low temperature *Cp* for films of CoO with different grain sizes, prepared by growing at different temperatures; data is plotted as *Cp/T* vs. T^2. These films weigh only a few micrograms and are measured using Si-micromachined calorimeters. As seen in the 7 nm bulk sample of nanocomposite-CoO, significant softening of the lattice (larger T^3 term and reduced Debye temperature) is seen in the film grown at room temperature compared to that grown at 100 °C. Also as seen in the nanocomposite-CoO, there is a small linear term in the data on the films that increases with decreasing grain size and is not present in the single crystal data.

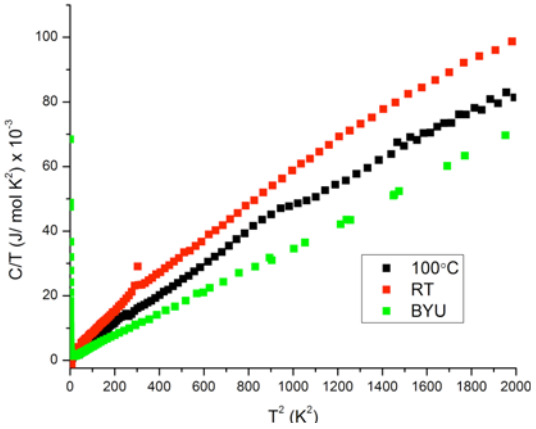

Figure 11 *Low temperature Cp for 300 nm thick CoO films grown at 100°C (average grain size from XRD 74 nm) and room temperature (average grain size 34 nm) compared to single crystal data. The small bump near 900 K^2 in one film reflects the antiferromagnetic ordering of a small amount of Co_3O_4 in this sample (on order of a few mol.%). Work at UCSD (films) and BYU (single crystal.)*

To further reduce grain size in the films, the specific heat of vapor deposited CoO films layered with amorphous SiO_2 (Figure 12a) was studied as a function of CoO layer thickness, as a comparison study to our earlier work [Abarra 1996] on CoO layered with MgO. The previous work with MgO intervening layers had shown broadening of the CoO peak, but very little suppression of the Néel temperature even for layers as thin as 1.6 nm (Figure 12b). The specific heat of CoO layers separated by SiO_2 demonstrates a dramatic difference. Here we see strong suppression and broadening, such that the material is not antiferromagnetic at any temperature for thicknesses below 2 nm. The explanation lies in the structure of the CoO layers: CoO/MgO grows as a coherent superlattice, with grains extending through the thickness of the film, which also results in large grain size in-plane, while for CoO/SiO_2, the amorphous nature of the intervening SiO_2 layers causes grain sizes to be strictly limited to the CoO thickness, causing the in-plane grain size to be similarly small (see Figure 5.1.3). For extremely thin CoO layers (< 2 nm), high resolution cross-sectional TEM images showed that the CoO was no longer structurally ordered but had become amorphous.

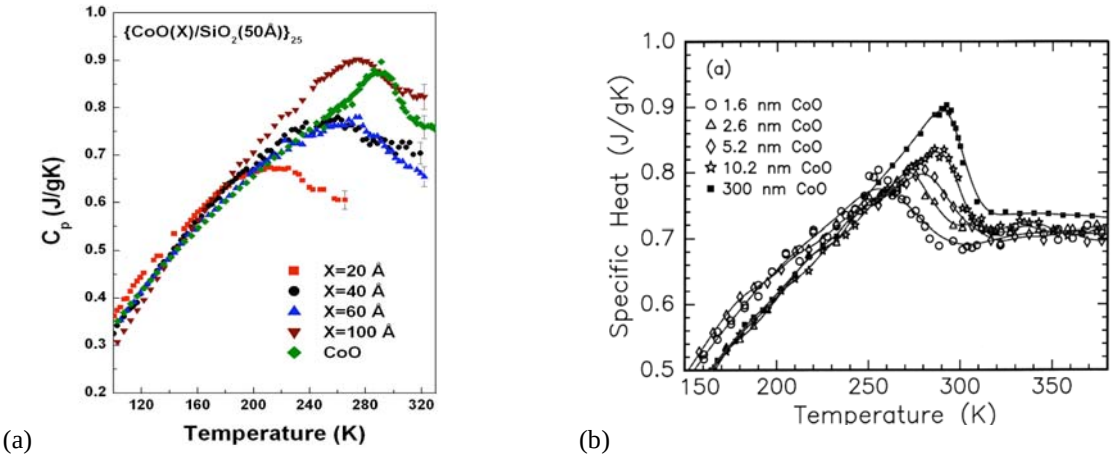

Figure 12(*a) Specific heat of CoO extracted from (CoO(X)/SiO$_2$(50 Å)$_{25}$ MLs with CoO thicknesses X = 20, 40, 60, and 100 Å, and for a 3000-Å CoO layer. For films with CoO layer thickness below 20 Å, the CoO is predominantly amorphous. Representative error bars are shown at one T for each.(b) Specific heat of CoO extracted from (CoO(X)/MgO(X)$_{25}$ MLs with CoO thicknesses X = 16, 26, 52, and 100 Å, and for a 3000-Å CoO layer (from [Abarra 1996]. Work at UCSD.*

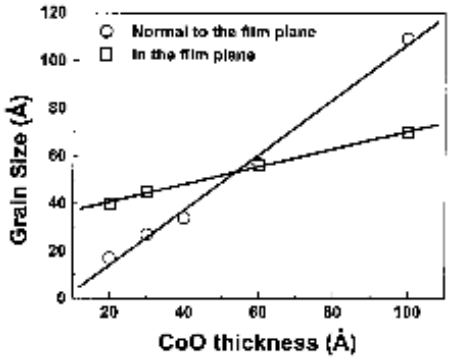

Figure 13 *Average grain size vs. CoO layer thickness: in-plane, □, from TEM images; normal to the film,* o, *from TEM and XRD. Work at UCSD.*

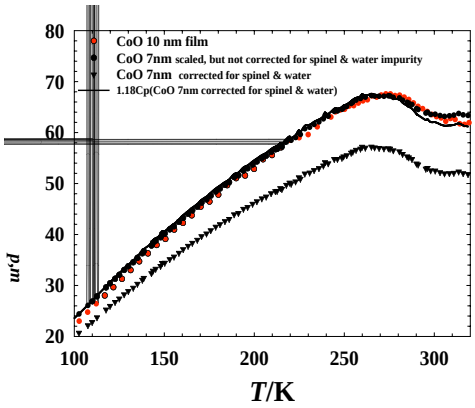

Figure 14 *Comparison of the nanoparticle and thin film CoO heat capacity. Nanoparticle data is shown with several scalings to illustrate shape agreement. Work at BYU and UCSD.*

It is instructive to compare the *Cp* of nanoparticles to that of films. Figure 13 shows that the 7 nm nanoparticle *Cp* bears a striking resemblance in peak shape and location of T_N to that of a CoO 10 nm film (in which grain sizes are 10 nm normal to the plane and 6 nm in plane, see Figure14). There is excellent agreement in magnitude if we compare the nanoparticle *Cp* before the water and Co_3O_4 corrections are applied. Multiplying the corrected nanoparticle results by 1.18 leads to a curve that is nearly superimposable on the film *Cp*. That the two results yields the same T_N and peak shape supports the notion that short-range order persists and controls the magnetic behavior for both films and nanoparticle materials.

Energetics of cobalt oxide nanoparticles and thin films

A series of CoO nanoparticles was synthesized by precipitation and thermal decomposition of cobalt hydroxides in a H_2/Ar atmosphere. We used temperature to control the particle size. The samples were characterized as described above for heat capacity measurements. The enthalpy of solution was measured using a CSC IMC 4400

calorimeter with HCl (5.0 N) as solvent at 25ºC. The enthalpy of solution of CoO nanoparticles was corrected for H_2O (assumed energetically equivalent to bulk liquid water) and excess oxygen (in the form of Co_3O_4). The excess enthalpies of the nanoparticles with respect to bulk CoO were calculated and plotted versus surface area from BET measurements (see Figure 15). A surface enthalpy of 2.82 ± 0.02 $J \cdot m^{-2}$ was obtained.

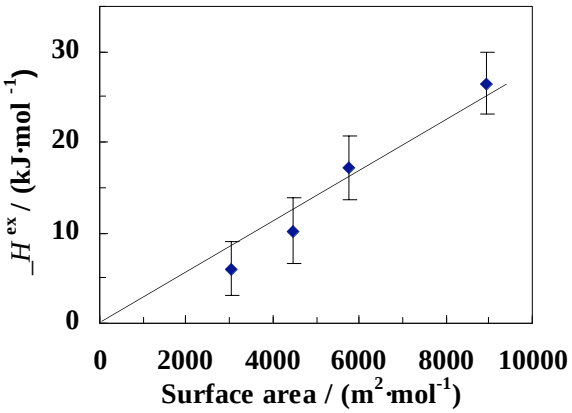

Figure 15. *Enthalpy of CoO nanoparticles relative to bulk CoO measured by solution calorimetry. The slope gives a surface enthalpy of 2.82 ± 0.02 $J \cdot m^{-2}$. Work at UCD.*

A CoO film of 1 μm thickness was prepared by reactive sputtering on Pt foils using a cobalt target in an argon/oxygen atmosphere; these films were grown at room temperature. The crystallite size calculated from XRD pattern is 56 ± 1 nm. SEM images show the grains have a prismatic shape and the average length of the base of the triangles (76 ± 3) nm. The TGA/DSC curves imply that the excess oxygen arises from the presence of Co_3O_4. The composition of the CoO film can be expressed as $CoO \cdot (Co_3O_4)_{0.012} \cdot (H_2O)_{0.039}$.

Thermogravimetry provided the water and oxidation state analysis. The Pt substrate was analyzed by electron microprobe and no Co/Pt alloy was found between the film and substrate. The Pt substrate itself contained negligible cobalt. Enthalpy of solution measurements was performed on a CSC IMC 4400 calorimeter with hydrochloride acid solvent at room temperature. After water and excess oxygen correction, the excess enthalpy of the film respect to bulk CoO is (7.00 ± 1.32) $kJ \cdot mol^{-1}$. This value includes the surface enthalpy of the film and interfacial enthalpy rising from the film-substrate interface and from grain boundaries in the film itself. Analysis in terms of surface and interfacial energies is underway.

CoO-MgO solid solutions

We began with a study of bulk materials. $Co_xMg_{1-x}O$ solid solution bulk samples were synthesized by solid-state reaction. The lattice parameters, within experimental limits of error, followed Vegard's Law. The compositions were determined by electron microprobe. The samples are homogeneous and close to the nominal compositions. The enthalpies of drop solution ($\Delta_{ds}H_m$) were determined by high temperature oxide melt calorimetry in molten sodium molybdate at 700°C. The measurements of heat capacity and magnetic transitions were conducted using an adiabatic calorimeter (below room temperature) and a differential scanning calorimeter (above room temperature).

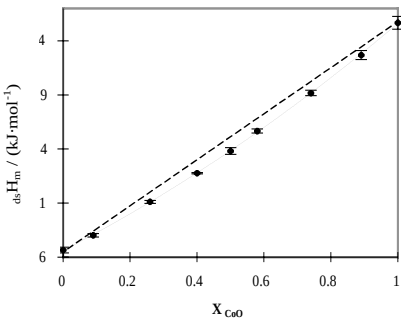

.**Figure 16.** *Enthalpy of drop solution ($\Delta_{ds}H_m$) of $Co_xMg_{1-x}O$ in sodium molybdate solvent at 973 K plotted against mole fraction CoO. The solid curve represents a quadratic fit to the experimental data*

The heat of drop solution, $\Delta_{ds}H_m$, is plotted as a function of composition in Figure 16. A symmetric curve, expressed by a quadratic equation, $\Delta_{ds}H_m$ / ($kJ \cdot mol^{-1}$) = (5.1 ± 0.3)x^2 + (15.9 ± 0.6)x – (5.4 ± 0.2), represents regular solution behavior relative to the end members, with a small positive enthalpy of mixing. From this measurement, the enthalpy interaction parameter is 5.1 ± 0.3 $kJ \cdot mol^{-1}$.

Heat capacities of $Co_{0.50}Mg_{0.50}O$ and end members were measured at 9 to 980 K. The standard entropy of the solid solution at 298.15 K, ignoring any configurational contribution, calculated from sub-ambient heat capacities is 40.2 ± 0.1 $J \cdot K^{-1} \cdot mol^{-1}$. From the difference between this quantity and the weighted sum of the entropies of the end-members, we obtain the excess (non-configurational) entropy, 0.2 ± 0.2 $J \cdot K^{-1} \cdot mol^{-1}$. Thus the nonconfigurational excess entropy is essentially zero.

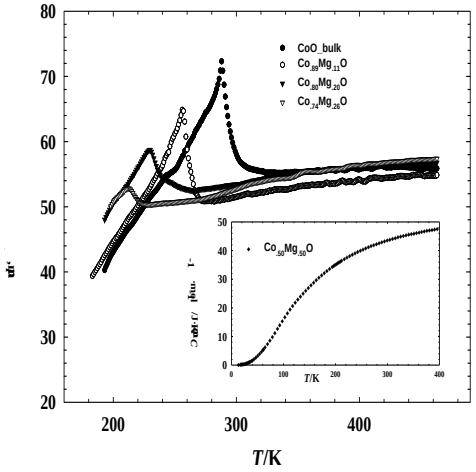

Figure 17. *Heat capacity curves of $Co_xMg_{1-x}O$ solid solutions obtained by DSC at UCD. Insert shows adiabatic calorimetry data from BYU.*

Figure 17 shows the heat capacity of $Co_xMg_{1-x}O$ solid solutions obtained by DSC. Although the data show a somewhat increased breadth of the magnetic transition with increasing dilution, the transitions are remarkably sharp, and compare quite favorably with literature data on $Co_xMg_{1-x}O$ [Seehra (1993)]. The excess heat content of $Co_{0.50}Mg_{0.50}O$ compared with end-members, from 298 K to 973 K, is 0.2 ± 0.2 kJ·mol^{-1}. Thus there is no excess entropy at higher temperatures and the heat of mixing does not depend on temperature.

We then turned to the study of CoO-MgO nanoparticles. $Co_xMg_{1-x}O$ solid solution for calorimetric measurements have been prepared with particle size of 30 - 100 nm by impregnation of freshly-prepared $Mg(OH)_2$ with Co nitrate, followed by thermal decomposition in pure N_2 at 900 ºC. The particle size grows when *x* increases. The surface area from BET is 2 – 35 m^2/g. TGA and electron microprobe analyses were performed. Additional characterization and calorimetry are in progress.